True Triaxial Strength Characteristics of Frozen Silty Sand

Haisheng Hong, Jie Zhu, Jie Wang
School of Civil Engineering, Anhui University of Science and Technology, Huainan, China

Abstract: The strength parameters of artificially frozen ground must consider the intermediate principal stress and temperature. Fengtai, Huainan remolded silty sand was tested under true triaxial tests at temperatures -5, -10 and -15 degrees Celsius. The lowest principal stress was 0.5, 1 or 2 MPa and the coefficient of intermediate principal stress b varied between 0 to 1. Failure stresses were measured as cohesion and friction angle, and failure stress ratio M was used to measure normalized strength response. Cohesion usually rose and then fell with b but the friction angle attained its highest tabulated value at b=0.75 at all three temperatures. Both parameters were raised by cooling at a constant b. Their varying behavior at high b indicates that ice bonding and resistance to friction cannot be captured in one enhancement factor. M had a peak at b=0.75 in all the temperature-confinement series and it grew with confinement, but its dependence on temperature was unlike that of cohesion and friction angle. A quadratic relation was fitted to describe the variation of MMM with bbb, with reported coefficients of determination greater than 0.95. Comparisons with the Drucker–Prager and FKZ criteria showed that the FKZ curves were closer to the experimental friction-angle curves for the selected cases. These results justify selection of temperature- and stress-state-dependent parameters for frozen walls in underground construction.

Keywords: Frozen Silty Sand; True Triaxial Test; Intermediate Principal Stress; Cohesion; Friction Angle; Failure Stress Ratio

1. Introduction

Silty sand is found in water-bearing strata when a mine-shaft is being sunk and other construction work underground. The engineering study of silty sand has to be considered as an issue that involves the compaction, particle interaction, and shear resistance [1]. It has also been interested in predicting strength of frozen silty sand since it alters the role of the pore water into the soil skeleton by freezing it [2]. A frozen wall will require that the ground be temporary structural support and prevent the flow of water through the wall. This means that the parameters of strength used in an excavation analysis have a direct influence on how load carrying capacity and choice of freezing scheme are evaluated.

Artificial freezing of the ground with water in it is a process that results in the creation of mineral particles, ice and unfrozen water. The mechanical reaction to excavation of artificial frozen sandy-gravelly formation has been studied [3]. The evolution of the field of temperature of freezing has also been analyzed depending on the direction of seepage [4]. These issues are related in the real world as the thermal state is dependent on the condition of material and the stress conditions change the stresses acting on the frozen ground when the excavation is done. Temperature and the stress situation at which failure occurs should be described in terms of strength.

The preparation of the material and history of the environment are important to understand the results of the frozen-soil tests. The effects of freezing-thawing, wetting-drying on modified soils have been studied in terms of mechanical characteristics and microstructure [5]. Researches of railway embankments in permafrost conditions have discussed the problem of water-thermal condition and its control [6]. In the mining areas, there is a weakly cemented water bearing strata that also raises some issues regarding time-dependent behavior of the mechanical properties [7]. These are the environmental and temporal responses of frozen ground. We will consider strength parameters of monotonic true triaxial loading.

The previous studies have studied the freezing-thawing and strength response of artificially frozen cement-treated soft clay [8], and numerical methods forecast stress-strain relationships of frozen-soil [9]. The temperature

Copyright @ STEMM Institute Press

and loading rate were also taken into account in sand behavior researches [10]. Loading paths to mechanical response have been shown to be relevant in work on confined materials [11]. In engineering scale, deformation of foundations and embankments in cold regions is influenced by material behavior and environmental conditions [12]. These results justify testing the strength of frozen-ground at controlled temperatures and loads.

The uniaxial analysis is a study that gives the details of temperature and strain-rate in frozen soils [13] whereas the traditional triaxial test can be used to determine the strength of granular soil mixtures [14]. This has been further extended by studies of frozen clay subjected to loading with complex stress paths to three-dimensional loading [15]. The examples of different loading conditions applicable to engineering practice are shown in the form of static and dynamic tests on silty sand [16]. Nevertheless, the traditional triaxial compression will apply the same amount of intermediate and minimum principal stresses. Such limitation cannot explain the whole state of stress that can be found surrounding an underground opening.

The difference can be studied by means of the middle principal stress. If we change the value of this stress, it will change the ratio of loading in the three directions even though the minimum stress is not changed. The variation in strength may affect both the cohesion intercept and the friction angle or one of them. The two effects are best considered separately so that they can explain the generalized strength response. By comparing the strengths, it will be possible to know which strength criterion has a better relation between its stress-state dependence and the observed response.

This paper presents an investigation into the true triaxial strength behaviour of remoulded frozen silty sand from Fengtai, Huainan. The analysis focuses on cohesion, friction angle and failure stress ratio at various temperatures, confining pressures and intermediate principal stress coefficients. Attention is drawn to the relative importance of bonding and friction, the behaviour close to the upper end of b*b*b, and the interpretation of normalised strength. The experimental friction-angle curves are then compared with the Drucker–Prager and FKZ criteria. The results are aimed at assisting with strength-parameter choice for frozen-ground analyses in underground construction.

2. Experimental Program

2.1 Soil and Specimen Preparation

The soil was the product of Block A of Phase IX of a resettlement project in Fengtai, Anhui Province, Huainan. The texture of the material was sandy and it was yellowish brown in color and non-plastic or very little plastic. Specimens dried were quite brittle. It is on similar silty sandy strata that are found in the mining region of Huainan. The specimens that were remolded were employed to regulate the preparation and the influence of temperature and 3D loading.

The soil was pulverized and filtered through a 1 mm sieve. It was dried to constant mass at 106 o C and mixed with distilled water to get a target water content of 16%. Water was applied uniformly while the soil was continuously mixed to reduce local accumulation and clumping. The water-content selection followed the compaction results in the experimental program. Physical testing and soil preparation were carried out with reference to the Standard for Geotechnical Testing Method, GB/T 50123–2019.

Cubic specimens of size 100×100×100mm100100100mm were made in a cleaned mould with a light coating of petroleum jelly on the internal surfaces to aid removal. The soil was placed in five layers, each roughened prior to placement of the subsequent layer. After levelling of the upper surface, the specimen and mould was frozen at −-20°C for 5 hours. The removed specimen was wrapped to minimise moisture loss and conditioned at the required temperature for 48 hours prior to testing.

2.2 Apparatus and Loading Procedure

The low-temperature true triaxial testing system was constructed by the collaboration of Anhui University of Science and Technology and Changchun Zhantuo Instruments Co., Ltd. The temperature control, hydraulic loading, and computerized control and data acquisition were incorporated into the apparatus. It had a range of -40 to 40 degrees Celsius in its temperature-control and claimed that it had an accuracy of +/-0.3 degrees Celsius. The three-dimensional unequal stresses on a cubic specimen could be applied with the help of independent control of the principal loading directions. In Figure 1 is presented the equipment that was used in the experimental programme.

 Copyright @ STEMM Institute Press



Figure 1. Low Temperature True Triaxial Testing Apparatus

The chamber was also pre cooled in the installation of specimens. When the specimen had been fixed, it was left at the desired temperature over a period of 2 h. The specimen was loaded by bringing the loading ends to touch the specimen and then applying isotropic load to the confining pressure that has been selected. This phase involved the application rate of force which was 20 N/s with an interval of 30 min. In shearing, the minor principal stress was not changed during the process but the major and intermediate principal loads were increased in a coordinated manner.

The major principal stresses are represented by 1, 2 and 3 with 1 = 2 = 3. The middle coefficient of the principal stress is b= (2 -3) / (1 -3). To ensure the required loading ratio was maintained, the nominal major and intermediate loading rates were 20 and 20b N/s respectively. In strain-softening responses, failure was determined by the maximum stress. In case of strain-hardening responses, the state of stress at a large principal strain of 15 percent was taken. These standards gave the failure stresses that were applied in the later calculations of parameters.

2.3 Test Conditions and Analysis Scope

The matrix of the experiments was a combination of three temperatures -5, -10 and -15 degrees Celsius, and three minimum principal stresses 0.5, 1 and 2 MPa. The b values were five, which are as follows: 0, 0.25, 0.50, 0.75, and 1.This is a 45 combinations of temperature and stress condition in the matrix. The two extreme values were intermediate-minimum equal and major-intermediate equal. Between these two extremes it was possible to test the effect of 2 sigma independently of the traditional triaxial compression state.

Two descriptions were employed in the strength analysis. The failure envelope of each temperature and b was given as cohesion and angle of friction which were used to give intercept and slope respectively. Failure stress ratio is an expression of the generalized shear stress against the mean principal stress at failure. All these values can be described by the fitted failure envelope and normalized stress state of failure. They are compared in terms of temperature, confinement and b under the monotonic loading conditions that have been prescribed.

3. Strength Parameters

3.1 Parameter Determination and Interpretation

Cohesion c and friction angle were determined by the major and minimum principal stresses at failure. At constant temperature and b, the three confining pressure results were employed to describe the relevant Mohr Coulomb envelope. The two values σ 1 -σ 3 give the largest difference in the principal stress and were taken as the tabulated parameters consistently. Maintaining b constant meant that each fitted envelope was one intermediate-principal-stress condition.

The values of c and 0 fitted represent failure within the range of confinement tested. The cohesion represents the intercept of the envelope and the friction angle determines its growth with normal stress. The contribution related to the ice-bonded structure is part of the intercept in frozen silty sand. The friction-angle term indicates the dependence of the resistance of the composite soil skeleton on stress. The two parameters are required in strength calculations since apparent cohesion and frictional resistance react differently to the loading condition.

Table 1 shows the parameters of the three temperatures. It is the same b values which are retained in each series and this is because the temperature effects can be compared at an equal stress state. The dependence on intermediate principal stress is shown in rows of each temperature series. In order to provide a shared reference point between the three temperature series, the b values were sampled with intervals of 0.25.

3.2 Cohesion Response to Temperature and Intermediate Principal Stress

Cohesion was normally found to rise with the

increase in b as it moved into the middle range and fell at a point of b=1. At -5 degrees Celsius, c was 0.97 MPa when b was 0 and increased to 1.41 MPa when b was 0.50 and reduced to 1.19 MPa when b was 1. The maximum tabulated values were 1.59 and 1.73 MPa respectively at -10 and -15 C, which were obtained at b=0.75. This change in cohesion intercepts was about 45, 51 and 43 percent higher than the original value at b=0.

The initial rise in cohesion is in line with increased constraint on the ice-bonded particle assembly as σ2subscriptσ2\sigma_ {2} increases compared to σ3subscriptσ3\sigma_ {3}. Under a more equilibrated three-dimensional stress state, relative particle motion and opening of local contacts may be inhibited. The frozen framework can support a higher failure-envelope intercept. The fitted cohesion represents resistance from both particles and ice and depends on stress path as well as temperature.

The high b decrease is a demonstration that the positive effect of increasing σ2subscriptσ2\sigma_ {2} is not uniform on the whole interval. The variation in the direction to b=1 alters the principal stress difference distribution and the deformation of the specimen as well. It can be resisted by confinement of one deformation direction and progressive destruction of the bonded structure. Cohesion is measured as the equilibrium between increased restriction and weakening of the ice bonds.

The high-b reduction also varied with temperatures. Between b=0.75 and 1, cohesion was reduced by 0.16, 0.15 and 0.17 MPa at -5, -10, and -15 o C respectively. The same absolute decreases took place in various initial levels of cohesion. By the time of -5 degrees Celsius, the decline had already started between b=0.50 and 0.75 but the colder series kept on increasing during this period. Therefore, temperature influenced not only the size of cohesion but also the form of its change with b. A common factor of improvement would not be able to reproduce all three series.

Cooling enhanced cohesion at all tabulated b. When the temperature was reduced to -5 and then to -15 o C, c increased by approximately 25 percent (0.97 to 1.21 MPa) at b=0. At b=0.75, this growth was 1.35-1.73 MPa or approximately 28%. The contribution of the frozen pore phase and the bonding between particles is reinforced with a lower temperature. This temperature response is isolated compared to variations in the proportions of the principal stress at the same b.

The increments of cooling were not the same in consecutive temperature ranges. The cohesion increased by 0.24 MPa at b=0.75 and by 0.14 MPa at -5 to -10 °C, and by 0.16 MPa at -10 to -15 °C. The corresponding increments at b=0 were 0.08 and 0.16 MPa. The cohesion increments thus rely on both temperature and b. The series should be interpolated at the relevant b because the thermal increment varies with stress state.

The practical value of the cohesion trend is contingent on its contribution to the failure envelope. A rise in intercept offers an extra contribution at a particular normal stress, and this is especially true when the frictional term is relatively low. Table 1 has already incorporated the combined effects of temperature and b into the values of cohesion. Further enhancement factors applied on these values would be counted twice in the measured gain.

Table 1. Cohesion and Friction Angle at Various Temperatures and b*b*b Values

b	−5 ℃ c/MPa	−5 ℃ φ/(°)	−10 ℃ c/MPa	−10 ℃ φ/(°)	−15 ℃ c/MPa	−15 ℃ φ/(°)
0	0.97	29.64	1.05	32.6	1.21	33.9
0.25	1.13	35.2	1.33	38.56	1.5	40.41
0.5	1.41	39.1	1.5	40.28	1.68	42.13
0.75	1.35	40.28	1.59	42.98	1.73	45.6
1	1.19	40.18	1.44	42.2	1.56	43.5

3.3 Friction Angle Response and its Relationship to Cohesion

Friction angle was also observed to increase at the three temperatures between b=0 and b=0.75 and then reduce slightly at b=1. At -5 degree Celsius, it rose to 40.28 degrees, 32.60 degrees, and 33.90 degrees respectively. The increments were 10.64 o, 10.38 o, and 11.70 o. This indicates that frictional part of the fitted envelope and its cohesion intercept were influenced by the intermediate principal stress.

The increase in 0 means that the stress-dependent contribution to shear resistance is stronger across the tested confinement range. The intermediate principal stress variation

 Copyright @ STEMM Institute Press

increases contact constraints and freedom of the granular skeleton to rearrange during shear. These variations may affect the frictional and interlocking factors which are indicated by the fitted angle. Both the intercept and slope of the failure envelope varied with b increasing. Cohesion due to ice alone thus cannot account on the measured response.

The response of the friction-angle was flattened around the upper end of b. At 0.75 to 1, phi reduced by only 0.10 degrees at -5 degrees Celsius compared with 0.78 degrees at -10 degrees Celsius and 2.10 degrees at -15 degrees Celsius. The warmest series thus tended towards a plateau while the coldest series exhibited a more pronounced decrease. The differences close to b=1 can be used to determine whether a strength criterion reproduces the high-b response.

The difference between c and 0 is especially evident at -5 o C. In the range of b=0.50 to 0.75, cohesion reduced by 1.41 to 1.35 MPa and friction angle rose by 39.10 degrees to 40.28 degrees. These opposing variations modify various parts of a single failure envelope. The increase or decrease in shear resistance as a result depends on the normal stress under which the envelope is assessed. Therefore, the maximum cohesion does not determine the highest resistance at each level of applied stress.

Cooling enhanced the value of φ at all b as it did cohesion. The angle changed by 4.26 between -5 and -15 o C when b=0. When b=0.75, there was an increase of 5.32 degrees. A more powerful ice-bonded structure can alter the circumstances in which the particles mobilize stress-dependent resistance, hence thermal effect goes beyond the intercept. There is a fitted envelope to every combination of temperature and b. One such angle would be measured using conventional triaxial compression without this variation.

The paired parameters must be kept together in the calculation of strength. An envelope can be formed by combining a maximum c of one b with a maximum φ of another, which was not measured under any condition. This problem occurs when the parameters are chosen at varying temperatures. In the case of frozen-wall calculation, c and 0 ought to be a common thermal and stress-state condition. The relationship between bonding and stress-dependent shear resistance is maintained by using a matched pair.

3.4 Failure Stress Ratio

The ratio of generalized shear stress q to mean principal stress p at failure is called the failure stress ratio M:

$$M = \frac{q}{p} \tag{1}$$

Table 2. Ratio of Failure Stress M at Various Temperatures and Confining Pressures (σ_3 in MPa)

b	−5 °C 0.5	−5 °C 1	−5 °C 2	−10 °C 0.5	−10 °C 1	−10 °C 2	−15 °C 0.5	−15 °C 1	−15 °C 2
0	0.91	1.06	1.22	0.90	0.99	1.15	0.86	0.96	1.12
0.25	1.18	1.29	1.41	1.14	1.25	1.31	1.12	1.20	1.33
0.5	1.42	1.49	1.61	1.36	1.46	1.55	1.32	1.41	1.50
0.75	1.54	1.62	1.73	1.50	1.56	1.68	1.49	1.55	1.66
1	1.50	1.58	1.69	1.46	1.51	1.63	1.42	1.50	1.59

In this case, p and q are given in MPa and M is dimensionless. The mean principal stress defines the general level of compressive stress and q defines the deviatoric part. Failure states can be compared using the ratio q/p on a normalized scale without losing their temperature, confinement, and b dependence. Table 2 contains all combinations tested. In every temperature category, the columns represent σ 3=0.5, 1, and 2 MPa.

M was found to rise with b=0.75 and fall at b=1 at all temperatures and confining pressures. Indicatively, when b=0, M was 0.91 and at b=0.75, it rose to 1.54 and reduced to 1.50. The values were 1.12, 1.66, and 1.59 at -15 o C and σ 3 =2 MPa. This trend was observed in all nine series with an intermediate-principal-stress effect on the normalized failure response being consistent.

The rise was also more significant in the lower-confinement series when it is stated in relation to the b=0 value. At -5 o C, with b increasing by zero to 0.75, M increased by about 69% at 0.5 MPa and 42% at 2 MPa. The normalized stress ratio at b=0 was already greater in the higher-confinement condition. Therefore, relative increment that goes with b must be differentiated with absolute level of M. An increase in percentage is not always accompanied by the highest final M.

Copyright @ STEMM Institute Press

M was found to increase with the minimum principal stress at constant temperature and b. When 0.50 and -10 C, M increased to 1.36, 1.46 and 1.55 as 0.5, 1 and 2 MPa were applied to 3 respectively. The same sequence happened in the entire table. Normalization of failure stresses did not eliminate their dependence on confinement. Therefore, M must be related to confining pressure as well as temperature and b.

The sensitivity to confinement also changed with b. At -5 o C, the increase of 0.5 to 2 MPa in σ3 led to an increase of M by 0.31 at b=0 and 0.19 at b=0.75. The effect of increasing confinement was thus added on a varying intermediate-principal-stress response. A comparison on one b cannot be extrapolated onto another by a constant additive increment. The comparison of matched series isolates the confinement response and the principal stress proportions effect.

Temperature generated another ordering of M compared to c and 0. At b=0.75 and =2 MPa, at -5 o C, M was 1.73 which reduced to 1.68 at -10 o C and 1.66 at -15 o C. The difference between the warmest and the coldest conditions was approximately 4 percent. However, cohesion and friction angle were observed to increase with cooling at this b. This distinction is based on the quantities that are being compared: M is a ratio between two measures of failure-state whereas c and phi define the fitted envelope in stress space. A lower M under cooling is not sufficient to determine a lower absolute failure stress. The ratio can be reduced when the mean stress and generalized shear stress change at different relative rates. M should thus be interpreted with dimensional failure stresses and envelope parameters. Cooling increased c and φ but decreased normalized ratio, so the three quantities give different rankings of the temperature response.

The quadratic relation was the observed rise and fall response:

$$M_b = Ab^2 + Bb + C \quad (2)$$

The parameters A, B and C are dimensionless regression coefficients and M_β is the ratio of b. The regressions gave R 2 values greater than 0.95 in the tested conditions. The relation explains the increase and decline of M in the sampled interval. Its coefficients must be linked to the temperature and confinement of the fitted series as Table 2 indicates variations in both the level of the baseline and the size of the b response.

The shared maximum at b=0.75 means that a quadratic representation should be able to capture the initial increase and subsequent reduction. Interpolation between measured points can then connect the discrete test conditions to intermediate stress states in an engineering calculation. The coefficients are specific to the temperature and confinement of each series, and the fitted relation is valid within the tested interval, 0≤b≤1.

3.5 Joint Interpretation and Implications to Frozen-Wall Analysis

The three parameters indicate the variation of intermediate principal stress on the fitted failure envelope and the normalized failure state. Cohesion and friction angle were normally improved with an increase in b in the low-to-intermediate range. They then behaved high-b, especially in the warmest series. M was able to integrate the failure stresses into a dimensionless quantity and had a constant sampled maximum. The difference between bonding, frictional resistance, and normalized failure stress is made by using all three parameters.

The temperature and the stress condition of a frozen wall in the case of a mine shaft can be different. The set of parameters must be determined according to the conditions that exist at the location where the calculation is made. It may be useful to divide the wall into regions by the temperature and then calculate the proportion of the main stresses in each region. Then, it will give the parameters for a three-dimensional analysis of strength without the coldest test values being applied to the warmest parts of the wall.

The representation of strength is what will decide the way in which these trends in the experimental results enter an engineering model. It is possible to calculate a Mohr-Coulomb with matched c-phi values and one that has a criterion with an explicit intermediate-principal-stress dependence can be used to reflect the variation of the failure surface more clearly. M may be considered as another comparison factor when verifying the normalized response in various loads. The tables of parameters explain the temperature and stress-state dependence, the test of the criterion is the ability of the mathematical formulation to reproduce it.

 Copyright @ STEMM Institute Press

4. Comparison of Strength Criteria

The dependence of the friction angle on b*b*b was employed for comparing the DP and FKZ criteria with the experimental response. This concerns the representation of the intermediate principal stress missing from a conventional envelope given only in terms of the major and minimum stresses. The DP criterion gives a commonly admitted three-dimensional formulation and the FKZ relation is another description of the friction-angle variation. The following expressions are tested against the experimental friction-angle curves

The relation that is related to the DP criterion can be expressed as follows:

$$\sin\varphi_b = \frac{3\sin\varphi_0}{3\lambda + (1-2b-\lambda)\sin\varphi_0} \tag{3}$$

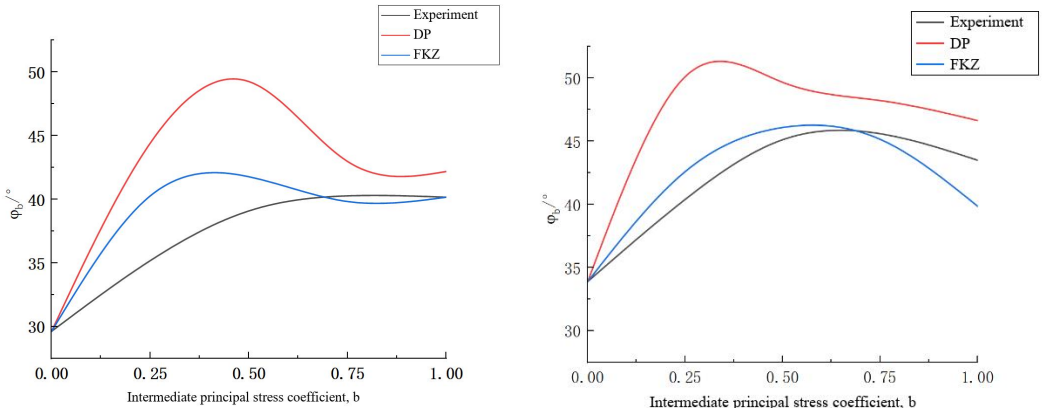
The corresponding FKZ relation is:

$$\sin\varphi_b = \frac{\sin\varphi_0}{\sqrt{1-b+b^2}} \tag{4}$$

In this case, phi o is the friction angle at b=0 and phi b is the friction angle at the given b. Auxiliary parameter lambda is defined below:

Where $\lambda = \sqrt{1-b+b^2}$

The Figure 2 is a comparison of the curves between the two chosen temperatures, -5 and -15 oC. The two panels cover the maximum and minimum temperature in the test matrix as well as the behavior across the entire b interval. It compares the reaction of friction-angle to various proportions of principal stress. The cohesion response related to it will be explained independently in section 3.



(a) −5 °C (b) −15 °C

Figure 2. The Friction-Angle Curves: (a) -5 C; (b) -15 C

The DP curves in the plotted comparison were above the experimental curves in most of the intermediate b range. Their high curvature suggested a more intense enhancement of the intermediate-principal-stress than that observed experimentally. This difference is pertinent since fitting the conventional triaxial condition does not guarantee that other parts of principal stress space would agree. The criterion of strength under unequal principal stresses is tested by the intermediate b values.

The FKZ curves were nearer to the experimental curves in general in the chosen panels. The difference was plotted at -5 o C and it became comparatively small towards the higher-b region. The FKZ curve was more similar to the experimental trend than the DP curve at −15 o C over most of the intermediate range. There were some differences close to the upper endpoint. FKZ provided the graphical agreement that is closer in these instances, but calibration must be extended to the entire b interval.

The criterion comparison is also informed by the parameter analysis in Section 3. Agreement on friction angle does not mean that predicted shear resistance will be same when cohesion varies. This problem can be demonstrated directly by separate sampled maxima of c and at −5 °C. The b dependence of the friction angle as well as the corresponding cohesion should be retained in a frozen-ground strength calculation; angular comparison alone lacks the envelope intercept.

The magnitude of the friction-angle predicted and b value at its maximum will have to be tested separately. A criterion that can give a good idea about the overall size, but not necessarily the greatest intermediate-stress effect, is possible to represent in terms of different b. There are five points in common where the tests are used to examine this matter with both ends. The curve shape is relevant to the interpolation between the sampled stress states as the experimental variation near the top end of the b is gradual. To interpolate between the measured states of stress, there has to be agreement over the interval.

Copyright @ STEMM Institute Press

The underground construction has a path to the three dimensional strength description, as the comparison of the experimental parameters. The b dependence that is measured will be used in testing a candidate criterion of stress states around the excavation. The current findings are related to remolded frozen silty sand at the specified monotonic load paths. In case of a specific frozen wall, such parameters can be verified through tests on the soil of the project at the appropriate temperature levels.

5. Conclusions

The strength parameters of remolded frozen silty sand were represented by true triaxial tests at three temperatures, three confining pressures and five intermediate principal stress coefficients. The analysis was done on cohesion, friction angle and failure stress ratio, and the experimental friction-angle curves were compared with two three-dimensional strength criteria. The key results are as below.

(1) Cohesion is usually increasing and then decreasing as a function of b. Its maximum tabulated value was at b=0.50 and -5 ° C, as well as at 0.75 and -10 and -15 degrees Celsius. At all the three temperatures, friction angle had its highest tabulated value at b=0.75. The parameters increased when cooled at every b. Their high-b reaction differences explain why one should consider temperature and stress state together in choosing a c-phi pair.

(2) M increased to b=0.75 and then declined in all the nine temperature -confinement series. With constant temperature and b, more confinement resulted in a greater M. Cooling decreased M even though cohesion and friction angle were increased showing that normalized and dimensional strength descriptions are different. The quadratic relations reported with R 2 above 0.95 offer an empirical description in the tested interval.

(3) The selected graphical comparisons revealed closer agreement between the FKZ and experimental friction-angle curves than between the DP and experimental curves. Selection of the criterion should also take into consideration the corresponding cohesion response. The results offer experimental input for assessing the stress-state-dependent strength of similarly frozen silty sands in mine-shaft and underground construction, where parameter selection is related to the corresponding temperature and loading condition.

References

[1] Yuan P, Hao J, Qi S, et al. Application of the sand-cone method in testing highway subgrade compaction. Soil Engineering and Foundation, 2026, 40(3): 584–587.

[2] Zhao N, Wang S, Wang L, et al. Prediction of the shear strength of frozen silty sand using Boosting, Bagging, Stacking, and Voting ensemble learning models. Journal of Glaciology and Geocryology, 2026, 48(2): 606–615.

[3] Zhang P, Yang C, Du X, et al. Mechanical response during tunnel excavation in artificially frozen sandy–gravelly strata. Chinese Journal of Underground Space and Engineering, 2026, 22(3): 1013–1022, 1033. DOI: 10.20174/j.JUSE.2026.03.27.

[4] Chen J, You Z, Zhou Y. Development of freezing temperature fields under different seepage directions. Journal of Railway Science and Engineering, 2026, 23(2): 821–832. DOI: 10.19713/j.cnki.43-1423/u.T20251109.

[5] Li J. Effects of freezing–thawing and wetting–drying cycles on the mechanical properties and microstructure of biopolymer-treated dispersive soil. Dissertation. Changchun: Jilin University, 2025. DOI: 10.27162/d.cnki.gjlin.2025.005097.

[6] Wang K. Hydrothermal characteristics and regulation methods for high-speed railway embankments in high-latitude discontinuous permafrost regions. Dissertation. Harbin: Harbin Institute of Technology, 2024. DOI: 10.27061/d.cnki.ghgdu.2024.003237.

[7] Wang Z, Yao Z, Zhang H, et al. Creep characteristics of water-bearing weakly cemented Jurassic sandstone in western mining areas. Journal of Jiamusi University (Natural Science Edition), 2025, 43(9): 67–70. DOI: 10.20232/j.cnki.jmsdxxb.2025.09.012.

[8] Wang S, Zhang X, Zhou B, et al. Freezing–thawing and strength characteristics of artificially frozen cement-treated soft clay. Journal of East China University of Technology (Natural Science), 2024, 47(4): 370–380.

[9] Yao Z, Liu J, Wang X. Prediction of the stress–strain relationship of artificially frozen soil using a KOA-LSTM model. Journal of Jiamusi University (Natural

 Copyright @ STEMM Institute Press

Science Edition), 2026, 44(4): 113–116, 82. DOI: 10.20232/j.cnki.jmsdxxb.2026.04.016.

[10] Jariyatatsakorn K, Kongkitkul W, In P Y. Temperature- and rate-dependent stress–strain–time behavior of sands and its simulation using a modified nonlinear three-component model. Arabian Journal for Science and Engineering, 2026, advance online publication: 1–24. DOI: 10.1007/s13369-026-11378-9.

[11] Hashim M Y, Qiao Fei Yang, Peng Da Li. Load path dependence for passively and actively confined high-strength concrete. Construction and Building Materials, 2024, 440: 137353. DOI: 10.1016/j.conbuildmat.2024.137353.

[12] Quan L, Tian B, Li S, et al. Driving factors and climate resilience of highway embankment deformation in permafrost regions of the Qinghai–Tibet Plateau. Journal of Traffic and Transportation Engineering, 2025, 25(5): 38–52. DOI: 10.19818/j.cnki.1671-1637.2025.05.003.

[13] Liang J, Hu X, He L, et al. Temperature and strain-rate effects on the uniaxial mechanical behavior and constitutive relationship of frozen soil. Journal of Disaster Prevention and Mitigation Engineering, advance online publication: 1–12, accessed August 10, 2026. DOI: 10.13409/j.cnki.jdpme.20251103001.

[14] Fan M, Liu C, Qiao Z, et al. Triaxial shear characteristics of sand–red clay mixtures and validation of the Duncan–Chang model. Journal of Jiamusi University (Natural Science Edition), 2026, 44(7): 87–90, 156. DOI: 10.20232/j.cnki.jmsdxxb.2026.07.009.

[15] Cao Y, Rong C, Wang Y, et al. Mechanical response and constitutive modeling of frozen calcareous clay under complex stress paths. Rock and Soil Mechanics, 2025, 46(7): 2071–2084. DOI: 10.16285/j.rsm.2024.1265.

[16] Shen C, Wang W, Zhong J, et al. Experimental study of the static and dynamic properties of silty sand at the Jiuweigang sluice-station project site. Jiangsu Water Resources, 2024, (7): 47–52. DOI: 10.16310/j.cnki.jssl.2024.07.016.

Copyright @ STEMM Institute Press